# Hydrodynamic and Interfacial Origin of Phase Segmentation in Solvent Extraction/Flow Injection Analysis

**Frederick F. Cantwell* and Jamal A. Sweileh**

*Department of Chemistry, University of Alberta, Edmonton, Alberta, Canada T6G 2G2*

**A semiquantitative physicochemical model is developed for the process by which alternating segments of aqueous and immiscible organic phases are produced at the confluence of streams of the two liquids. A growing "drop" of one phase is dislodged to produce a segment when the hydrodynamic force exerted on it as a result of flow of the other solvent is equal to the interfacial force holding it in place. Hydrodynamic forces are expressed by Poiseuille's and Bernoulli's laws while interfacial force is expressed by a form of the Tate equation in terms of liquid–liquid interfacial tension and solid–liquid–liquid contact angle.**

Solvent extraction performed in the flow injection analysis (FIA) mode requires that two immiscible solvent streams undergo a confluence at some sort of segmentor from which they emerge into an extraction coil as alternating segments of the two phases, typically organic, O, and aqueous, A (*1*, *2*). In all systems in which flow rates of the confluent streams are maintained constant and uninterrupted, the volumes of the O and A segments, and hence their lengths in the extraction coil, are governed by a combination of hydrodynamic and interfacial forces. It is the purpose of this report to establish the theoretical basis for understanding the segment-forming process and to test the resulting model experimentally. The segmentor design employed is based on a simple "tee" made of Kel-F which has been used successfully in several applications of solvent extraction/FIA (*1–3*), but the underlying theory will apply, with suitably modified parameters, to all constant flow segmentors.

## EXPERIMENTAL SECTION

**Apparatus.** Solvents were pumped by two liquid chromatography pumps (Model 6000A, Waters Assoc., and Mini-Pump Model 396, Laboratory Data Control) to ensure constancy of flow rates. The solvents met in the "tee" segmentor shown in Figure 1. Attached to the exit of the segmentor was a 300 cm long coil of 0.8 mm i.d. Teflon tubing which served as the extraction coil. Segment length in the extraction coil was studied as a function of flow rate. To do this both pumps were first set to identical flow rates and pumping was continued for several minutes. The two pumps were then turned off at the same time, and the lengths of the stationary segments were measured near the downstream end of the extraction coil. Solvents were not preequilibrated before being pumped to the segmentor. Teflon inserts, consisting of short segments of 0.8 mm i.d. tubing, were placed in three branches of the tee to improve the regularity of segmentation as discussed below (see Figure 1).

**Solvents.** Reagent-grade chloroform and methyl isobutyl ketone (MIBK) were used as received. Water was distilled, deionized, and distilled from alkaline permanganate.

**Contact Angles.** Solid–liquid–liquid contact angles, $\theta$, were measured in a 4 cm long by 0.16 cm i.d. capillary machined from Kel-F. They were measured for MIBK/$H_2O$ and for $CHCl_3$/$H_2O$ by the capillary rise technique (*4*, *5*).

## RESULTS AND DISCUSSION

**Contact Angles.** The solid–liquid–liquid contact angle, $\theta$, is related to the height of the capillary rise, $h$, by the expression (*5*)

$$\cos\theta = \frac{\Delta\rho g h r}{2\gamma_{o/w}} \quad (1)$$

where $\Delta\rho$ is the density difference between the organic solvent and water, $\gamma_{o/w}$ is the liquid–liquid interfacial tension between organic and aqueous phases, $g$ is the gravitational constant, and $r$ is the radius of the measurement capillary. In the 0.079 ± 0.001 cm radius capillary used, the MIBK/$H_2O$ interface was depressed by 1.2 ± 0.08 cm and the $CHCl_3$/$H_2O$ interface was elevated by 1.7 ± 0.06 cm, which gives cos $\theta$ of 0.88 ± 0.06 and 0.98 ± 0.04, respectively, for MIBK/$H_2O$ with $\gamma_{o/w}$ of 10.7 dyn/cm (*6*) and for $CHCl_3$/$H_2O$ with $\gamma_{o/w}$ of 32.8 dyn/cm (*7*). For MIBK/$H_2O$, $\theta$ = 29 ± 7°. In $CHCl_3$/$H_2O$, $\theta$ = 11° as an average value, but, because of the closeness of cos $\theta$ to 1, the range of $\theta$ within the experimental uncertainty of cos $\theta$ is 0–20°. The fact that a larger value of $\theta$ is observed for a solvent system with a smaller value of $\gamma_{o/w}$ is consistent with observations on other hydrophobic solids at low $\gamma_{o/w}$ (*8*).

**Segmentation.** The phase segmentor differs from those used in earlier studies (*1*, *2*) by the inclusion of short inserts of 0.08 cm i.d. Teflon tubing in the three branches of the tee. In their absence, irregular segmentation patterns sometimes developed in which usually long and short segments appeared. This was observed to be due to creeping of the organic phase along the wall into the aqueous inlet branch of the tee where it formed an adherent droplet located a millimeter or two into the branch. The droplet grew in size until it formed a constriction large enough to occasionally facilitate breakage of the aqueous stream at that point rather than at the junction of the three branches of the tee where it normally occurs. Inclusion of the Teflon tubing inserts in the tee eliminated the problem over a wide range of flow rates. With $F_o/F_A$ maintained at 1.0, the lengths of the aqueous and organic segments are necessarily equal when segmentation is regular.

The experimentally measured dependence of segment length $L$ on total flow rate $F_T$ is shown in Figure 2A for $CHCl_3$/$H_2O$ and in Figure 2B for MIBK/$H_2O$ over the ranges of $F_T$ where segmentation is regular. At higher $F_T$ than those shown, the segmentation patterns were regular at the segmentor but were irregular at the measurement point as the result of coalescence of segments during passage through the extraction coil. It is evident from Figure 2 that shorter segments are produced at higher flow rates and that, at a given flow rate, longer segments are obtained with MIBK/$H_2O$ then with $CHCl_3$/$H_2O$.

These two features of the $L$ vs. $F_T$ curves are a consequence of the physical processes responsible for segment formation at the tee, which can be described in the following terms by reference to Figure 3. The vertical and horizontal orientation of the branches of the tee in Figure 3 are merely for ease of reference in the following discussion. Gravity probably plays

0003-2700/85/0357-0329$01.50/0 

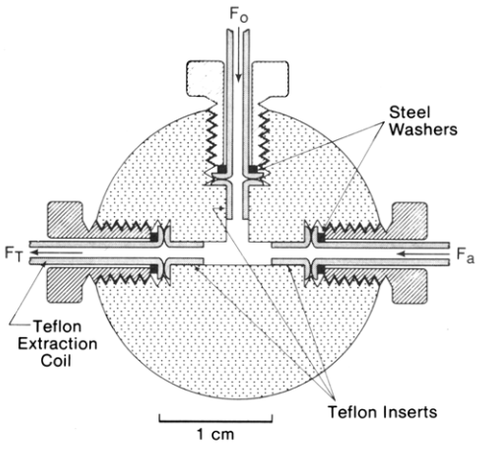


**Figure 1.** Diagram of the Kel-F segmentor tee showing the Teflon inserts and upstream end of the extraction coil. $F_A$ = water flow rate, $F_o$ = organic flow rate, $F_T$ = total flow rate.

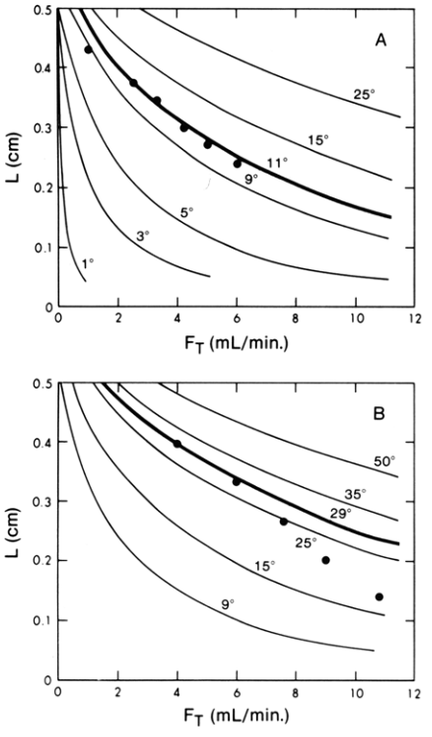


**Figure 2.** Segment length vs. total flow rate for chloroform–water (A) and methyl isobutyl ketone–water (B). $F_o/F_A$ = 1. Points are experimental and lines are theoretical for the contact angles shown.

a negligible role in the segment forming process. As shown in Figure 3A, the flow of organic solvent phase (O) into the aqueous phase (A) flow stram has the appearance of a drop of O. It should be realized, however, that since the diameters of the vertical and horizontal branches of the tee are equal, the sides of the drop of O are in contact with the side walls of the horizontal branch at the junction of the tee. This is shown in the end view in Figure 3D where the growing drop of O is seen to descend like a gate across the aqueous flow stream. A hydrodynamic force is exerted on the drop of O as a result of the perpendicular flow of A. This force tends to dislodge (break off) the drop of O from the column of O above and "slide" it along the surface of the left horizontal branch of the tee. The drop will be dislodged in this way when the *hydrodynamic force* pushing it is equal to the *interfacial force* holding it onto the vertical column of O. When the drop of O finally is dislodged and moves into the horizontal branch, it tends to minimize its contact area with A and maximize its

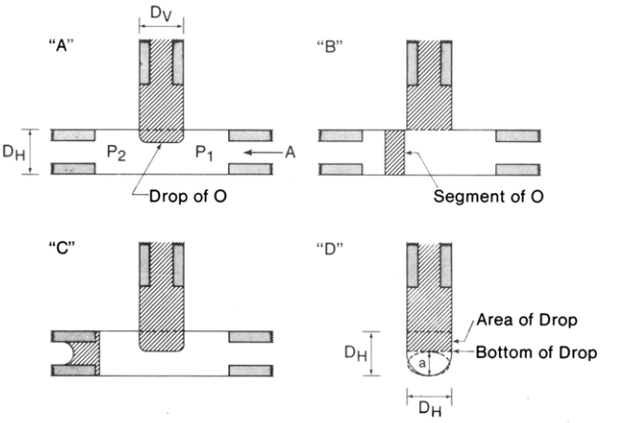


**Figure 3.** Diagram of segment formation at the "tee". A–C are side views, D is end view of tee. Organic phase is shaded (see text for details). $P_1$ and $P_2$ are upstream and downstream pressures across the drop of the organic phase.

contact area with the Kel-F wall, on which it is a wetting solvent. This results in a rearrangement of the dislodged drop to form a segment of O (Figure 3B) which subsequently is pushed along into the 0.8 mm i.d. Teflon insert and extraction coil (Figure 3C).

Before providing quantitative descriptions of the hydrodynamic and interfacial forces involved, several assumptions of the model should be clarified: (i) Because both O and A are always flowing there will continue to be flow of O into the drop during the time that it is dislodging. It is assumed in subsequent calculations that once the drop has started to dislodge it does so very rapidly, so that the volume of O flowing into it during the transition from drop to segment (Figure 3A to 3B) is negligible. (ii) Visual observation of the tee at very slow flow rates showed that spreading of O along the walls of the horizontal branches did not occur during drop growth (before dislodgment). It can safely be assumed that such spreading does not occur at the flow rates used in Figure 2 since they are even closer to the critical jetting velocity (*9*). (iii) The drop is assumed to growth straight down, along the extrapolated axis of the vertical branch. In fact, visual observation at very low flow rates, where drops grow to a large size before dislodging, shows that they bend somewhat toward the left (downstream). Presumably this drop distortion occurs to some extent at all flow rates, but it will be neglected in calculating the hydrodynamic force. (iv) The effects of the Teflon inserts in the tee on flow streamlines, especially in the upstream horizontal branch, are ignored (*10–13*). (v) To facilitate calculations, the cross section of the space below the growing drop is assumed to be elliptical, as shown in Figure 3D, with its major axis equal to the diameter of the horizontal tube ($D_H$ = 0.16 cm) and its minor axis, $a$, equal to the difference between $D_H$ and the vertical length of the drop at any time. Vertical drop length is calculated from the geometry of the space at the crossing point of the tee into which the drop is growing and from $F_o$ and time. Use of $D_H$ as the major axis is justified by the fact that the largest segment length observed in the experiments reported in Figure 2 corresponds to $a > D_H/2$, so that the meniscus never got further than about the position shown in Figure 3D. (vi) Interfacial tensions and contact angles were measured on preequilibrated phases, while the liquids pumped in the segmentation studies were not preequilibrated.

Segment formation is quantitatively described as follows: The hydrodynamic force tending to dislodge the drop is the product of the area of the drop facing the aqueous stream (AR; Figure 3D) times the pressure difference across the drop due

to the aqueous flow ($\Delta P = P_1 - P_2$; Figure 3A). Drop area may be expressed in terms of $L$ as

$$AR \cong \frac{D_H \pi L D_c^2}{4 D_v^2} \tag{2}$$

where $D_c$ and $D_v$ are the internal diameters of the extraction coil (0.08 cm) and the vertical branch of the tee (0.16 cm), respectively. The pressure difference $\Delta P$ is composed of two contributions: The first arises from the viscous drag on the aqueous phase as it flows through the elliptical "capillary tube" beneath the organic phase drop, and the second arises from the kinetic energy loss of the aqueous phase flowing through the same elliptical "orifice". The relationship of $\Delta P$ to volumetric flow rate $F_A$ through a short elliptical tube is given as a combination of Poiseuille's law and Bernoulli's law by the following expression (*13*)

$$\Delta P \cong \frac{F_A 8 \eta_A (D_v + 1.64R)}{\pi R^4} + \frac{1.12 \rho_A F_A^2}{\pi^2 R^4} \tag{3}$$

in which $\eta_A$ is the viscosity of A, $\rho_A$ is the density of A, and $R$ is the equivalent radius of the ellipse (*13*) given by

$$R \equiv \frac{a^2 D_H + a D_H^2}{2a^2 + 2 D_H^2} \tag{4}$$

The minor axis of the ellipse can be calculated from

$$a = D_H - \frac{\pi L D_c^2}{4 D_v^2} \tag{5}$$

The hydrodynamic force $f_{HYD}$ exerted by the flow of A on the growing drop of O is given by

$$f_{HYD} = AR \Delta P \tag{6}$$

The drop will be dislodged when this force equals the interfacial force holding the drop onto the column of O.

The interfacial force is the force required to take an area of $\pi(D_v/2)^2$ of O which is on contact with the vertical column of O and move it into contact with the Kel-F wall. This interfacial force $f_{INT}$ is given by the following form of the Tate equation (*4*, *5*):

$$f_{INT} = 2\pi(D_v/2)\gamma_{O/A}(1 - \cos\theta) \tag{7}$$

The value of $f_{INT}$ is independent of drop size. It is thus evident in a qualitative way that when a larger aqueous flow rate $F_A$ is used, $f_{HYD}$ will be equal to $f_{INT}$ at a smaller drop size so that, as is seen experimentally, $L$ is smaller at higher $F_A$. A quantitative expression for $F_A$ in terms of $L$ can be obtained by substituting $f_{INT}$ from eq 7 for $f_{HYD}$ in eq 6 and combining the result with eq 2–5. Since $D_H$, $D_v$, and $D_c$ are known from the design of the system, $\eta_A$ and $\rho_A$ can be looked up in tables, $a$ and $R$ can be calculated for any value of $L$, and $\theta$ has been measured experimentally for $CHCl_3/H_2O$ and for MIBK/$H_2O$; it is possible to calculate the values of $F_A$ expected for various values of $L$. $F_T$ is readily obtained from

$$F_T = F_A + F_O \tag{8}$$

where $F_O = F_A$ in this case.

The solid *points* in Figure 2 show the experimentally measured dependence of $L$ on $F_T$. The *lines*, calculated via eq 2–8 for various assumed values of $\theta$, are theoretical predictions. The two dark lines are the theoretical predictions for $CHCl_3/H_2O$ ($\theta = 11°$, $\gamma_{O/A} = 32.8$ dyn/cm) and MIBK/$H_2O$ ($\theta = 29°$, $\gamma_{O/A} = 10.7$ dyn/cm) based on their experimentally measured $\theta$. The remarkably good fit of the experimental points to the theoretical line for $\theta = 11°$ in the $CHCl_3/H_2O$ system must be considered to be somewhat fortuitous in light of the large experimental uncertainty in $\theta$ for the system. For both of the solvent systems the experimental points describe more nearly straight lines than are predicted by the hydrodynamic interfacial model. A substantial discrepancy between theory and experiment is not surprising in view of the simplifying assumptions (i)–(vi) that were necessary. However, the model does predict the main features of the data—the decrease of $L$ with increasing $F_T$ and the displacement of the MIBK/$H_2O$ curve to higher $L$ than the $CHCl_3/H_2O$ curve (the latter being mainly a consequence of the larger contact angle for Kel-F/MIBK/$H_2O$). The proposed semiquantitative model represents a viable basis for a theoretical understanding of the segmentation process and will serve as a guide in the design of new and modified segmentors in continuous flow systems.

It may be noted, in this connection, that in segmentors designed around a jet in which the drop grows and breaks off in such a way that it is not in contact with the wall at the time of dislodgment, then cos $\theta$ is absent from eq 7. The resulting equation for $f_{INT}$ would have the more conventional form of the Tate equation (*4*, *5*) which corresponds to very much higher values of $f_{INT}$ for a given jet diameter ($D_v$) than those encountered in the tee segmentor.

## ACKNOWLEDGMENT

Hubert Hoffman of the Chemistry Department machine shop fabricated the Kel-F capillary.

## LITERATURE CITED

(1) Fossey, L.; Cantwell, F. F. *Anal. Chem.* **1982**, *54*, 1693.
(2) Fossey, L.; Cantwell, F. F. *Anal. Chem.* **1983**, *55*, 1882.
(3) Sweileh, J. A.; Cantwell, F. F. *Anal. Chem.*, in press.
(4) Davies, J. T.; Rideal, E. K. "Interfacial Phenomena", 2nd ed.; Academic Press: New York, 1963; Chapter 1.
(5) Adamson, A. W. "Physical Chemistry of Surfaces", 2nd ed.; Interscience: New York, 1967; Chapters 1 and 7.
(6) Keith F. W., Jr.; Hixon, A. N. *Ind. Eng. Chem.* **1955**, *47*, 258.
(7) "International Critical Tables", 1st ed.; McGraw-Hill: New York, 1928; Vol. 4, pp 432–475.
(8) Peper, H.; Berch, J. *J. Phys. Chem.* **1964**, *68*, 1586.
(9) Hayworth, C. B.; Treybal, R. E. *Ind. Eng. Chem.* **1950**, *42*, 1174.
(10) Drew, T. B.; Dunkle, H. H.; Genereaux, R. P. In "Chemical Engineer's Handbook", 3rd ed.; Perry, J. H., Ed.; McGraw-Hill: New York, 1950; Chapter 5.
(11) Daniels, F.; Williams, J. W.; Bender, P.; Alberty, R. A.; Cornwell, C. D. "Experimental Physical Chemistry", 6th ed.; McGraw-Hill: New York, 1962; Chapter 8.
(12) Partington, J. R. "An Advanced Treatise on Physical Chemistry"; Longman: New York, 1951; Vol. 1, pp 881–887.
(13) Partington, J. R. "An Advanced Treatise on Physical Chemistry"; Longman: New York, 1951; Vol. 2, pp 72–80.

RECEIVED for review May 31, 1984. Accepted August 17, 1984. This work was supported by the Natural Sciences and Engineering Research Council of Canada and by the University of Alberta.